



Testing Feedback-regulated Star Formation in Gas-rich, Turbulent Disk Galaxies

D. B. Fisher¹, A. D. Bolatto², H. White³, K. Glazebrook^{1,4}, R. G. Abraham³, and D. Obreschkow⁵¹Centre for Astrophysics and Supercomputing, Swinburne University of Technology, P.O. Box 218, Hawthorn, VIC 3122, Australia²Laboratory of Millimeter Astronomy, University of Maryland, College Park, MD 29742, USA³Department of Astronomy & Astrophysics, University of Toronto, 50 St. George St., Toronto, ON M5S 3H8, Canada⁴ARC Centre of Excellence for All-sky Astrophysics (CAASTRO), Australia⁵International Centre for Radio Astronomy Research (ICRAR), M468, University of Western Australia, 35 Stirling Hwy., Crawley, WA 6009, Australia

Received 2018 July 26; revised 2018 October 25; accepted 2018 November 2; published 2019 January 4

Abstract

In this paper we compare the molecular gas depletion times and midplane hydrostatic pressure in turbulent, star-forming disk galaxies to internal properties of these galaxies. For this analysis we use 17 galaxies from the DYNAMO sample of nearby ($z \sim 0.1$) turbulent disks. We find a strong correlation, such that galaxies with lower molecular gas depletion time (t_{dep}) have higher gas velocity dispersion (σ). Within the scatter of our data, our observations are consistent with the prediction that $t_{\text{dep}} \propto \sigma^{-1}$ made in theories of feedback-regulated star formation. We also show a strong, single power-law correlation between midplane pressure (P) and star formation rate surface density (Σ_{SFR}), which extends for 6 orders of magnitude in pressure. Disk galaxies with lower pressure are found to be roughly in agreement with theoretical predictions. However, in galaxies with high pressure we find P/Σ_{SFR} values that are significantly larger than theoretical predictions. Our observations could be explained with any of the following: (1) the correlation of $\Sigma_{\text{SFR}}-P$ is significantly sublinear; (2) the momentum injected from star formation feedback (p_*/m_*) is not a single, universal value; or (3) alternate sources of pressure support are important in gas-rich disk galaxies. Finally, using published survey results, we find that our results are consistent with the cosmic evolution of $t_{\text{dep}}(z)$ and $\sigma(z)$. Our interpretation of these results is that the cosmic evolution of t_{dep} may be regulated not just by the supply of gas but also by the internal regulation of star formation via feedback.

Key words: galaxies: evolution – galaxies: ISM – galaxies: starburst – galaxies: star formation

1. Introduction

The majority of star formation in massive galaxies occurred roughly 10 billion years ago, during the epoch $z \sim 1-3$ (Hopkins & Beacom 2006; Madau & Dickinson 2014). There are significant differences in the gas and star formation properties in those distant galaxies, compared to local universe spirals. The molecular gas fraction increases significantly from ~ 0 to $z \sim 3$ (e.g., Combes et al. 2013; Tacconi et al. 2013), while molecular gas depletion time, $t_{\text{dep}} \equiv M_{\text{mol}}/\text{SFR}$ (where SFR is the star formation rate), has a only modest decrease from ~ 2 Gyr at $z \approx 0$ (Bigiel et al. 2008; Saintonge et al. 2011; Leroy et al. 2012; Rahman et al. 2012) to $\sim 0.3-0.7$ Gyr at $z \approx 2$ (Tacconi et al. 2013; Genzel et al. 2015; Schinnerer et al. 2016; Scoville et al. 2016; Magdis et al. 2017).

The observed evolution of molecular gas depletion time is considerably shallower than predictions from simulations and semianalytic models (e.g., Davé et al. 2011; Lagos et al. 2015). These theories assume that the depletion time is mostly regulated by available gas supply and the cosmic evolution of the dynamical time. Alternatively, the slow evolution has been seen as evidence that local processes may determine gas depletion times (e.g., Genzel et al. 2015). Indeed, the internal properties of galaxies at higher redshift are observed to be very different. They have supergiant star-forming regions (Genzel et al. 2011; Guo et al. 2012; Wisnioski et al. 2012; Fisher et al. 2017b) and elevated gas velocity dispersions (Förster Schreiber et al. 2009; Lehnert et al. 2009; Swinbank et al. 2012; Wisnioski et al. 2015, e.g.). Recent high-resolution observations confirm predictions (e.g., Dekel et al. 2009; Genzel et al. 2011) that the properties of these giant star-forming regions, so-called “clumps,” are directly consistent with being the result of galaxy-wide disk instabilities (Fisher et al. 2017a; White et al.

2017; Dessauges-Zavadsky & Adamo 2018). We note that alternate theories do exist. For example, Inoue & Yoshida (2018) argue that clumps are consistent with forming via fragmentation of spiral arms, which are likewise consistent with data.

The elevated gas velocity dispersions in gas-rich galaxies are most commonly interpreted as signatures of strong, galaxy-wide turbulence. Some authors have interpreted this turbulence to be driven by star formation feedback (e.g., Green et al. 2010; Lehnert et al. 2013); however, the nature of the mechanism driving this turbulence remains under debate (e.g., Krumholz & Burkhardt 2016).

Ostriker et al. (2010) present a detailed model for star formation in which the vertical pressure is balanced by pressure-supporting mechanisms, such as energy injected from supernovae. In this model turbulence is driven primarily by feedback from supernova explosions. Models in which star formation feedback drives turbulence (also Faucher-Giguère et al. 2013) predict that in marginally stable systems the depletion time is inversely dependent on the vertical velocity dispersion (σ_z). Ostriker & Shetty (2011) also predict that the SFR surface density should be directly proportional, or at least nearly proportional (Shetty & Ostriker 2012; Kim et al. 2013), to the midplane pressure of the galaxy disk. In essence the pressure from the galaxy is supported by the energy injected from feedback processes associated with star formation. If the depletion time is indeed linked to the internal kinematics, this may give an explanation for the slow cosmic evolution of t_{dep} , as it would be regulated not just by gas inflow but also by feedback processes.

Krumholz et al. (2012) present an argument in which the turbulence is driven by gravitation alone. They argue that

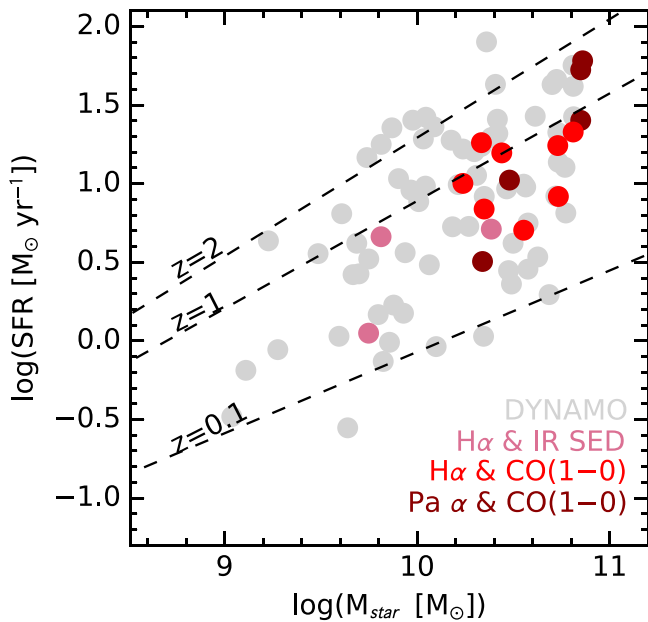


Figure 1. SFR is plotted against stellar mass for galaxies in our sample. The color of data points indicates the data type used to determine the SFR and the gas mass. We also plot as dashed lines the main sequence of galaxies at three different redshifts, $z = 0.1$, 1, and 2. Main-sequence values are taken from Speagle et al. (2014). DYNAMO galaxies span the range in SFR– M_* from $z > 0.1$ to $z \leq 2$.

feedback is not necessary to describe the bulk properties of star formation in galaxies. Krumholz & Burkhardt (2016) argue that galaxies follow a linear correlation such that $\text{SFR} \propto \sigma$, albeit with significant scatter, which is predicted in this theory. These models predict a very different dependence of depletion time. In this case, t_{dep} is most affected by the dynamical time of the galaxy (similar to Davé et al. 2011; Lagos et al. 2015) and has either no dependence on velocity dispersion or a positive dependence. Different models of turbulence-driving mechanisms therefore predict very different parameter dependencies with t_{dep} .

Heretofore, these direct predictions have remained difficult to test owing to a lack of sufficient range in parameters. For example, σ is effectively constant across well-studied samples of nearby galaxies, like THINGS (Leroy et al. 2008). Observations of higher-redshift galaxies would provide larger dynamic range in properties like midplane pressure, molecular gas depletion time, and σ . However, with present facilities the signal-to-noise ratio (S/N) of internal properties of galaxies is low and introduces both a significant amount of scatter to correlations and a selection bias toward larger, brighter targets.

We use the DYNAMO sample (Green et al. 2010, 2014) of rare galaxies located at $z = 0.075$ – 0.2 that have properties very similar to turbulent, clumpy disk galaxies more commonly found at higher redshift.

Throughout this paper, we assume a concordance cosmology with $H_0 = 67 \text{ km s}^{-1} \text{ Mpc}^{-1}$, $\Omega_M = 0.31$, and $\Omega_\Lambda = 0.69$.

2. Sample and Data Sources

2.1. DYNAMO Sample

The galaxies considered here are a subset of the DYNAMO survey galaxies Green et al. (2014). DYNAMO galaxies are selected from Sloan Digital Sky Survey (SDSS) DR4 based on high $\text{H}\alpha$ line flux, while excluding active galactic

nuclei (AGNs) from the sample. In Figure 1 we show that the galaxies in our sample have specific SFRs (SFR/M_*) that range from the low- z main-sequence values to those of $z \approx 1$ – 2 . The sample spans $M_{\text{star}} = (0.9$ – $9) \times 10^{10} M_\odot$, $\text{SFR} \sim 1$ – $60 M_\odot \text{ yr}^{-1}$, and extinction $A(\text{H}\alpha) \sim 0.2$ – 1.7 mag . Overall, galaxies similar to those in DYNAMO-*HST* are extremely rare in the local universe, with a space density of $\sim 10^{-8}$ to 10^{-7} Mpc^{-3} .

A number of observational results have been published showing that DYNAMO galaxies are more similar to $z \approx 1.5$ main-sequence galaxies than local universe ultraluminous infrared galaxies (ULIRGs). DYNAMO galaxies have very high molecular gas fractions, $f_{\text{gas}} \approx 0.2$ – 0.8 (Fisher et al. 2014; White et al. 2017), whereas local universe galaxies typically have molecular gas fractions of less than 10%. White et al. (2017) show that unlike local universe ULIRGs, DYNAMO galaxies have lower dust temperatures ($T_{\text{dust}} \sim 20$ – 30 K).

An important similarity of DYNAMO galaxies to $z \sim 1$ – 2 main-sequence galaxies is in the kinematics. DYNAMO galaxies are rotating systems with high gas velocity dispersions, $\sigma \sim 20$ – 100 km s^{-1} (Green et al. 2010, 2014; Bassett et al. 2014; Bekiaris et al. 2016). Observations with $\sim 100 \text{ pc}$ resolution confirm that these high dispersions are not caused by beam-smearing effects (Oliva-Altamirano et al. 2018). Moreover, Bassett et al. (2014) show that these kinematic signatures are also observed in the stellar kinematics of DYNAMO galaxies, thus indicating that it is not likely a gas disk inside a system of stars with different kinematics. Finally, Obreschkow et al. (2015) show that the angular momentum of DYNAMO galaxies is low for disks of their stellar mass but is very similar to what has since been observed in $z \approx 1.5$ main-sequence galaxies (Swinbank et al. 2017).

Using *Hubble Space Telescope* (*HST*) $\text{H}\alpha$ maps, Fisher et al. (2017b) show that DYNAMO galaxies are “clumpy,” and when DYNAMO images are degraded to match $z \approx 2$ observations, they meet quantified definitions of clumpy galaxies (e.g., Guo et al. 2015). Moreover, Fisher et al. (2017a) show that those DYNAMO galaxies identified as “disks” meet detailed predictions of Toomre (1964) instability theories, whereas control galaxies identified as mergers do not. Specifically, they find that the size of clumps correlates with the kinematics of disks, and clumps are only found in annuli that are unstable by the Toomre analysis.

Overall, the properties of DYNAMO galaxies most closely resemble galaxies at $z \approx 1$ – 2 . DYNAMO galaxies are therefore excellent laboratories for studying the processes in clumpy, turbulent disks with higher resolution and greater sensitivity.

In this analysis we only include targets that are identified as “disk galaxies.” We use the same criteria as described in Fisher et al. (2017b) that disk galaxies both show rotating ionized gas in 2D velocity fields and are well fit by an exponentially decaying surface brightness profile. For surface photometry we use the FR647M continuum images for galaxies imaged with *HST* and the $1.9 \mu\text{m}$ continuum for galaxies observed with OSIRIS. For the galaxy G10-1 we use 500 nm continuum from GMOS for the stellar surface brightness profile, which has 1.2 kpc resolution. Galaxies G03-2, D00-2, and C14-2 only have SDSS imaging to measure the stellar surface brightness profile, which is considerably poorer resolution. However, all three of these galaxies have measured dust temperatures from *Herschel* data of 20–30 K (White et al. 2017), which

Table 1
Sample Properties

Galaxy	z	M_{star} $10^{10} M_{\odot}$	M_{mol} $10^9 M_{\odot}$	Kinematic Source ^a	SFR $M_{\odot} \text{ yr}^{-1}$	$R_{1/2}$ kpc	Emission Line ^a	Gas Source ^a
C14-2	0.0562	0.56	1.83 ± 0.36	WiFeS ³	1.12 ± 0.17	4.0	H α ³	IR SED ³
D00-2	0.0813	2.43	5.08 ± 0.84	WiFeS ³	5.14 ± 0.72	3.5	H α ³	IR SED ³
G03-2	0.12946	0.65	5.16 ± 1.18	WiFeS ³	4.6 ± 0.89	4.5	H α ³	IR SED ³
G10-1	0.14372	2.75	13.45 ± 2.15	GMOS ³	15.7 ± 1	1.2	H α ³	CO (1-0) ³
D20-1	0.07049	2.95	5.93 ± 0.65	WiFeS ³	4.7 ± 0.25	3.4	H α ³	CO (1-0) ³
G04-1	0.12981	6.47	29.00 ± 2.10	GMOS ²	21.32 ± 1	2.8	H α ²	CO (1-0) ¹
G20-2	0.14113	2.16	5.22 ± 0.59	GMOS ²	18.24 ± 0.35	2.1	H α ²	CO (1-0) ³
D13-5	0.07535	5.38	11.90 ± 0.36	GMOS ²	17.48 ± 0.45	2.0	H α ²	CO (1-0) ¹
G08-5	0.13217	1.73	7.11 ± 0.79	GMOS ²	10.04 ± 1	1.8	H α ²	CO (1-0) ³
D15-3	0.06712	5.42	9.36 ± 0.18	WiFeS ²	8.29 ± 0.35	2.2	H α ²	CO (1-0) ³
G14-1	0.13233	2.23	4.94 ± 0.59	GMOS ²	6.9 ± 0.5	1.1	H α ²	CO (1-0) ³
C13-1	0.07876	3.58	5.91 ± 0.15	WiFeS ²	5.06 ± 0.5	4.2	H α ²	CO (1-0) ³
C22-2	0.07116	2.19	4.94 ± 0.35	OSIRIS ⁴	3.2 ± 0.28	3.4	Pa α ⁴	CO (1-0) ⁵
SDSS 024921-0756	0.153	3.02	7.30 ± 0.56	OSIRIS ⁴	10.54 ± 1.054	1.1	Pa α ⁴	CO (1-0) ⁵
SDSS 212912-0734	0.184	7.08	51.15 ± 3.77	OSIRIS ⁴	53 ± 5.3	1.3	Pa α ⁴	CO (1-0) ⁵
SDSS 013527-1039	0.127	7.08	34.89 ± 1.61	OSIRIS ⁴	25.27 ± 2.527	1.6	Pa α ⁴	CO (1-0) ⁵
SDSS 033244+0056	0.182	7.24	40.32 ± 2.39	OSIRIS ⁴	60.5 ± 6.05	1.9	Pa α ⁴	CO (1-0) ⁵

Note.^a References. (1) Fisher et al. 2014; (2) Fisher et al. 2017a; (3) White et al. 2017; (4) Oliva-Altamirano et al. 2018; (5) this work.**Table 2**
Derived Properties of Sample Galaxies

Galaxy	σ (km s^{-1})	V_{flat} (km s^{-1})	t_{dep} (Gyr)	Σ_{SFR} ($\log(M_{\odot} \text{ yr}^{-1} \text{ kpc}^{-2})$)	P/k_B ($\log(\text{cm}^{-3} \text{ K})$)	P_{DE}/k_B ($\log(\text{cm}^{-3} \text{ K})$)
C14-2	26	159	1.63 ± 0.41	-2.254 ± 0.093	4.63 ± 0.42	4.96 ± 0.37
D00-2	35	61	0.99 ± 0.21	-1.464 ± 0.089	5.47 ± 0.28	5.80 ± 0.21
G03-2	32	189	1.12 ± 0.34	-1.751 ± 0.106	4.91 ± 0.41	5.27 ± 0.31
G10-1	52	117	0.86 ± 0.15	-0.094 ± 0.071	7.64 ± 0.24	7.96 ± 0.15
D20-1	35	134	1.26 ± 0.15	-1.500 ± 0.032	5.56 ± 0.21	5.89 ± 0.17
G04-1	50	269	1.36 ± 0.12	-0.650 ± 0.030	6.94 ± 0.16	7.26 ± 0.13
G20-2	81	166	0.29 ± 0.03	-0.482 ± 0.023	6.45 ± 0.18	6.82 ± 0.13
D13-5	46	192	0.68 ± 0.03	-0.475 ± 0.024	6.86 ± 0.14	7.18 ± 0.12
G08-5	64	243	0.71 ± 0.11	-0.628 ± 0.048	6.67 ± 0.19	7.04 ± 0.13
D15-3	45	240	1.13 ± 0.05	-0.867 ± 0.028	6.61 ± 0.13	6.94 ± 0.12
G14-1	70	136	0.72 ± 0.10	-0.358 ± 0.038	7.33 ± 0.19	7.68 ± 0.14
C13-1	29	223	1.17 ± 0.12	-1.644 ± 0.048	5.27 ± 0.25	5.60 ± 0.20
C22-2	32	164	1.54 ± 0.17	-1.647 ± 0.044	5.45 ± 0.25	5.78 ± 0.19
SDSS 024921-0756	57	84	0.69 ± 0.09	-0.135 ± 0.061	7.58 ± 0.16	7.91 ± 0.13
SDSS 212912-0734	53	105	0.97 ± 0.12	0.411 ± 0.061	8.56 ± 0.16	8.82 ± 0.13
SDSS 013527-1039	41	232	1.38 ± 0.15	-0.110 ± 0.061	7.88 ± 0.16	8.14 ± 0.13
SDSS 033244+0056	59	239	0.67 ± 0.08	0.134 ± 0.061	7.81 ± 0.14	8.11 ± 0.13

Note. Uncertainty on σ is 3–5 km s^{-1} and on V_{flat} is 5–10 km s^{-1} .

strengthens the case that they are disk-like systems rather than major mergers. These three targets are plotted as different color points in all results figures. As discussed in Fisher et al. (2017b), galaxies H10-2 and G13-1 do not meet the criteria of disks, and from Oliva-Altamirano et al. (2018) galaxy E23-1 does not meet this definition of a disk galaxy.

For our analysis we make observations to measure molecular gas masses, ionized gas maps with ~ 100 pc resolution, and kinematics of ionized gas. We present gas masses and kinematics on 17 DYNAMO galaxies, and we obtain ionized gas maps for 13 targets. All of these methods are well tested and have been used on the DYNAMO sample in previously published works. Here we summarize the basics of each.

2.2. Gas Masses

We compile CO (1–0) observations from Fisher et al. (2014) and White et al. (2017) using the Plateau de Bure Interferometer (PdBI) and the Northern Extended Millimeter Array (NOEMA), respectively, with new NOEMA observations.

New NOEMA observations were made during the period 2016 May–December, with observing programs S16CK and W16BK (PI: Fisher). We use the same observational method and similar measurement techniques as were previously published in Fisher et al. (2014) and White et al. (2017). Similar to previous observations (Fisher et al. 2013; White et al. 2017), all observations were made with the WIDEX correlator. These observations comprise six of the targets listed in Table 1.

Table 3
CO Observations

Galaxy	Observation Date	Time on Target (hr)	Beam Size (arcsec ²)	$\nu_{\text{CO}}(\text{sky})$ (GHz)	Line Width (km s ⁻¹)	F_{CO} (Jy km s ⁻¹)	Source Source
G10-1	2013 Jun 11	1.0	5.86 × 4.55	100.786	358	1.6 ± 0.26	Fisher et al. (2014)
	2013 Jun 17	1.4					
D13-5	2013 May 30	1.8	6.32 × 3.54	107.194	334	10.04 ± 0.31	Fisher et al. (2014)
G04-1	2013 Jun 21	0.8	10.94 × 5.25	102.027	352	6.63 ± 0.48	Fisher et al. (2014)
	2013 Jul 16	0.8					
G20-2	2014 May 23	0.9	9.46 × 4.71	101.017	237	1.57 ± 0.18	White et al. (2017)
G08-5	2014 May 20	1.1	5.36 × 4.47	101.812	353	2.44 ± 0.27	White et al. (2017)
D15-3	2014 May 30	1.5	6.26 × 4.44	108.023	361	12.8 ± 0.25	White et al. (2017)
G14-1	2014 May 29	1.1	7.13 × 4.66	101.803	236	1.69 ± 0.2	White et al. (2017)
C13-1	2014 May 20	1.1	5.94 × 4.19	106.851	196	5.84 ± 0.15	White et al. (2017)
C22-2	2016 Jul 19	1.9	34.87 × 2.73	107.613	240	2.77 ± 0.19	This Work
D20-1	2016 Jul 19	1.1	56.5 × 6.31	107.681	280	3.4 ± 0.37	This Work
SDSS 024921-0756	2016 Aug 15	2.2	5.3 × 3.16	99.975	300	2.42 ± 0.19	This Work
SDSS 212912-0734	2016 Jul 9	1.5	4.91 × 3.89	97.357	340	2.26 ± 0.16	This Work
	2016 Jul 10	3.8					
SDSS 013527-1039	2016 Dec 2	3.4	4.57 × 1.689	102.281	220	4.42 ± 0.2	This Work
SDSS 033244+0056	2016 Dec 10	1.9	3.39 × 2.17	97.522	460	1.83 ± 0.11	This Work

Typical integration times were 1–2 hr in C or D configurations. The correlator was tuned to observe the redshifted CO (1–0) emission line in each target. This yielded an on-sky frequency of 97–107 GHz for targets ranging in redshifts from 0.18 to 0.07. These observations were then calibrated using standard GILDAS routines in CLIC and then cleaned with the MAPPING pipeline routine during an on-site visit to IRAM. Observations were reduced with the default channel width of 20 km s⁻¹ and then binned to 50 km s⁻¹, yielding cubes with typical rms \sim 2–3 mJy. Final flux uncertainties for each target are given in Table 3.

Our targets are unresolved in these PdBI and NOEMA observations. Two of the sources (D20-1 and C22-2) have particularly elongated beams. However, these do not significantly affect the measurement of the flux. We have overlaid the beam shape and size on SDSS *r*-band images and checked each source for possible contamination from other sources. The only source with an additional source in the beam area is G20-2, which contains a point source representing less than 1% of the flux of G20-2 in the FR647M *HST* continuum image but is barely detectable in H α . It is, therefore, not likely that this is changing the CO flux by a significant amount.

The spectrum for each target is measured in a polygon region containing the galaxy. These spectra are shown in Appendix A. Fluxes are obtained by binning the data into 50 km s⁻¹ channels and then integrating the resulting spectrum. The choice in range of channels to integrate over is made by starting at the redshifted frequency of the CO (1–0) line and summing all adjacent channels that are above the noise limit. The total line widths of our targets are typically 300–400 km s⁻¹. Noise levels for the observations were in the range of 0.5–1.0 mJy. We also consider that the choice in how to measure flux may affect the final value. We therefore also measure flux by fitting a single-component Gaussian function to the data, as well as measuring the flux in 20 km s⁻¹ channels. We take the standard deviation of the four different fluxes for each target and add this in quadrature with the noise in the spectrum to estimate the measurement uncertainty of flux. This value is shown in each spectrum in Appendix A. The range of S/N for new NOEMA observations was S/N = 10–22. Observational details of CO detections are listed in Table 3.

The CO (1–0) flux is converted to molecular gas mass (M_{mol}) in the usual fashion, in which $M_{\text{mol}} = \alpha_{\text{CO}} L_{\text{CO}}$, where L_{CO} is the luminosity of CO (1–0) and α_{CO} is the CO-to-H₂ conversion factor, including a 1.36 \times correction for heavier molecules. We adopted the standard value $\alpha_{\text{CO}} = 4.36$. We have made multiple efforts to determine the most appropriate value of α_{CO} . First, based on SDSS spectra, DYNAMO galaxies have slightly subsolar metallicity. Recently, White et al. (2017) study the dust temperature for a set of DYNAMO galaxies, including several in this work. They find that DYNAMO galaxies have low dust temperatures, $T_{\text{dust}} \sim$ 20–30 K, implying Milky-Way-like conversion factors (as reviewed in Bolatto et al. 2013). Moreover, of the few galaxies that have both dust SED and CO (1–0) observations, the estimated gas masses agree to \sim 25%. Finally, Fisher et al. (2014) used the formula from Bolatto et al. (2013), which estimates α_{CO} via the baryonic surface density, and found a result consistent with the Milky Way value.

We also include three targets from White et al. (2017) for which the gas mass is determined from *Herschel* observations. Here we estimate the dust mass by fitting blackbody models to the infrared spectral energy distribution (SED) and then convert to molecular gas mass by assuming a constant dust-to-gas ratio, similar to other works (e.g., Genzel et al. 2015).

2.3. Star Formation Rates

Fisher et al. (2017b) present 10 *HST* H α maps of DYNAMO galaxies, using ramp filters FR716N and FR782N with the Wide Field Camera on the Advanced Camera for Surveys (WFC) on *HST* (PID 12977; PI Damjanov). Integration times were 45 minutes in the narrowband filter and 15 minutes with the continuum filter. All images were reduced using the standard *HST* pipeline. We correct the fluxes measured in the image using an [N II]/H α ratio determined from the SDSS spectrum for each target. Seven of the DYNAMO-*HST* sample galaxies also have CO (1–0) fluxes and are included here. A detailed description of the observations, continuum subtraction, and clump measurement is given in Fisher et al. (2017b). The typical resolution of DYNAMO-*HST* observations is 60–150 pc.

We also observed five galaxies with Pa α emission lines observed with Keck OSIRIS (Larkin et al. 2006). Our targets were observed with the laser guide star system with exposure times of 4×900 s, achieving resolution of 150–400 pc. We use the OSIRIS data reduction pipeline version 2.3. To flux-calibrate the OSIRIS spectra, we use the telluric stars observed each night (an average of three telluric stars per night). Our method corresponds to a first-order flux calibration consistent with the Two Micron All Sky Survey magnitudes within $\sim 20\%$. Detailed descriptions of both observation and reduction of OSIRIS data cubes are given in Bassett et al. (2017) and Oliva-Altamirano et al. (2018).

SFRs are calculated from the emission-line flux using the extinction-corrected H α line luminosity by assuming $\text{SFR} [M_{\odot} \text{ yr}^{-1}] = 5.53 \times 10^{-42} L_{\text{H}\alpha} [\text{erg s}^{-1}]$ (Hao et al. 2011). We calculate the intrinsic H α extinction using the H α and H β line ratios from SDSS spectra. For those targets with OSIRIS data we divide the Pa α luminosity by the intrinsic luminosity ratio, $L_{\text{Pa}\alpha}/L_{\text{H}\alpha} = 0.128$ (Calzetti 2001). Using H α fluxes from Green et al. (2017), we find that $\text{SFR}_{\text{H}\alpha} - \text{SFR}_{\text{Pa}\alpha} \approx \pm 2.5 M_{\odot} \text{ yr}^{-1}$.

Three galaxies in our sample have neither *HST* nor OSIRIS data. For these we use the published H α emission line fluxes measured from AAT/SPIRAL and AAT/WiFES (Green et al. 2017).

2.4. Kinematics

Data cubes containing intensity, velocity dispersion, and rotation velocity of each galaxy are extracted from the data by fitting Gaussian functions with point-spread function convolution to emission lines in individual spaxels. These are then fit with kinematic models by the method of least squares using the GPU-based software *gbkfit* (see Bekiaris et al. 2016). Inclination is taken from photometry. We model the rotation velocity, v_{rot} , with the function (Boissier et al. 2003)

$$v_{\text{rot}}(r) = v_{\text{flat}} [1 - \exp(-r/r_{\text{flat}})]. \quad (1)$$

The software then returns v_{flat} and r_{flat} .

The fit to the data cubes also includes an intrinsic component of velocity dispersion, σ . In the model the velocity dispersion is assumed to be constant across the disk. Fitting the velocity dispersion simultaneously in the model allows for accounting of the beam smearing in the data (Davies et al. 2011), as well as inclination. This flat velocity dispersion profile makes a necessary assumption that the galaxy is a disk and further requires our effort to exclude mergers as described above.

An alternative approach to modeling velocity dispersions is to make a weighted average of the velocity dispersion in the region of the galaxy that also shows a flat rotation curve. Oliva-Altamirano et al. (2018) investigate both methods with DYNAMO galaxies. They generate model galaxies designed to match clumpy DYNAMO disks. Then they fit these with both *gbkfit* and straightforward averages. They find that both methods recover similar values for velocity dispersion, with modeling being slightly more stable as it intrinsically accounts for rising dispersion in galaxy centers. On average the models and average methods have a difference of $\sigma_{\text{ave}} - \sigma_{\text{model}} \lesssim 5 \text{ km s}^{-1}$, which is consistent with our error bars.

The data sources for both σ and V include AAT/WiFES H α observations (Green et al. 2014), Keck OSIRIS observations of Pa α (Oliva-Altamirano et al. 2018), and Gemini GMOS

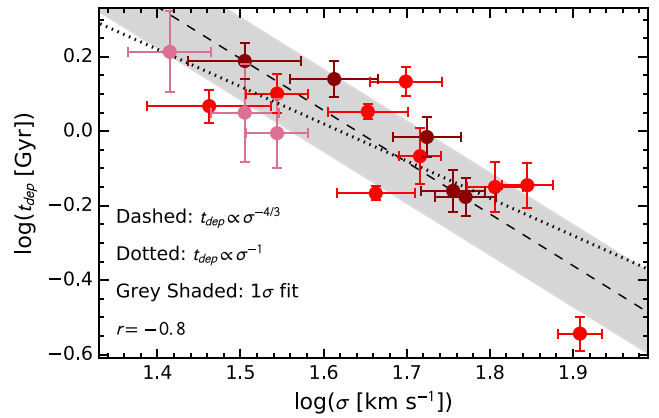


Figure 2. Relationship between galaxy depletion time and internal gas velocity dispersion. Symbol colors represent the source of data as described in Figure 1. The gray region indicates the 1σ scatter around the best-fit relation. The dashed line represents the prediction from multi-freefall turbulence models (Salim et al. 2015). The dotted line indicates the prediction from feedback-driven models (e.g., Ostriker et al. 2010). Indeed, we observe a strong negative correlation between t_{dep} and σ_{gas} .

observations of H α and H β (Bassett et al. 2014; Fisher et al. 2017a). For a more detailed description of Gemini observations see Bassett et al. (2014). In those cases in which multiple observations are made on a single target we preference first the GMOS observations, as this data set offers both deep, high-S/N observations and subkiloparsec resolution, then OSIRIS observations as a result of the high resolution, and then AAT observations. The kinematic parameters we use here, derived from the three separate data sets, are found to generally agree on the order of the uncertainties, $\sim \pm 5\text{--}10 \text{ km s}^{-1}$ (Bassett et al. 2014; Bekiaris et al. 2016; Oliva-Altamirano et al. 2018).

Properties derived for analysis in this work (including kinematics, molecular gas depletion time, and pressure) are listed in Table 2.

3. Molecular Gas Depletion Time in Turbulent Disks

In our sample we find a range of $t_{\text{dep}} = 0.3\text{--}1.6$ Gyr, with the average for our sample at 1 Gyr. This range in t_{dep} was the intended effect of targeting galaxies with a range in SFR/ M_* , as shown in Figure 1. Our observations reproduce the relationship⁶ between t_{dep} and the SFR/ M_* of Saintonge et al. (2011) of $t_{\text{dep}} \propto (\text{SFR}/M_*)^{-0.53 \pm 0.14}$ with Pearson’s correlation coefficient of $r = -0.6$. This correlation has also been observed in high-redshift galaxies (e.g., Tacconi et al. 2017). This continues to motivate our treatment of this DYNAMO sample, as well representing the properties of actively star-forming galaxies.

3.1. Relationship with Gas Velocity Dispersion

In Figure 2 we compare t_{dep} to velocity dispersion of ionized gas (σ). For reference, Wisnioski et al. (2015) find that σ_{gas} increases from $\sim 10\text{--}20 \text{ km s}^{-1}$ in the local universe to $\sigma > 30 \text{ km s}^{-1}$ at $z > 1$. In our sample, all galaxies with $t_{\text{dep}} < 1$ Gyr have $\sigma > 40 \text{ km s}^{-1}$.

Considering our entire DYNAMO data set, we find a strong, inverse relationship between the molecular gas depletion time and the gas velocity dispersion, with a Pearson’s correlation

⁶ Throughout this paper we measure parameter correlations using the maximum likelihood *R* package *Hyperfit* (Robotham & Obreschkow 2015).

coefficient of $r = -0.8$ and a p -value of 8.7×10^{-5} . The best-fit relationship for these quantities is

$$\log(t_{\text{dep}}) = -1.39 \pm 0.23 \times \log(\sigma) + 2.27 \pm 0.38, \quad (2)$$

where t_{dep} is in Gyr and σ is in km s^{-1} . The vertical scatter around this correlation is 0.12 Gyr. We note that in our data set this correlation has less scatter and a stronger correlation coefficient than that of t_{dep} and SFR/M_* .

To investigate how much the correlation depends on the galaxy with the largest velocity dispersion/shortest depletion timescale (G20-2), we remove it from the sample and recompute r and p . It is possible that this galaxy is at the least affecting the power law of the correlation to some degree. We therefore refit the data excluding galaxy G20-2. We still find a strong, inverse correlation for the data set that excludes this target, with a Pearson's correlation coefficient $r = -0.78$ and a p -value of 4.7×10^{-4} . The best-fit quantity for this subset of the data that does not include G20-2 is

$$\log(t_{\text{dep}}) = -1.04 \pm 0.20 \times \log(\sigma) + 1.71 \pm 0.33. \quad (3)$$

To be clear, the exclusion of G20-2 is a completely ad hoc treatment. We do not observe any special features of this target that lead us to believe that it is any more peculiar than the other DYNAMO galaxies. Fisher et al. (2017b) present both the $\text{H}\alpha$ map and 600 nm continuum surface brightness profile of all DYNAMO galaxies, and G20-2 does not have significant asymmetries, aside from the presence of clumps. Moreover, there are no detectable companion galaxies in the *HST* images. We do note that G20-2 has a very prominent ring with a radius of ~ 1 kpc. This may be driving a higher star formation efficiency or larger σ when compared to other DYNAMO galaxies. However, G04-1 and D13-5 both have rings as well, albeit less prominent than that of G20-2. We note that in Figure 4 of this work we will find that G20-2 is not an outlier.

As discussed in Robotham & Obreschkow (2015), the maximum likelihood fitting technique provides a robust treatment of uncertainties. Nonetheless, we also consider ordinary least-squares (OLS) bisector fits to the data. We do this to ensure that our fitting method is not somehow biasing the result. Also, OLS techniques have been in use for a much longer time (Isobe et al. 1990), allowing for standard comparison with previous work. We find that a fit to all our data recovers an OLS bisector of $t_{\text{dep}} \propto \sigma^{-1.30 \pm 0.18}$ and the fit to the data set in which G20-2 is omitted recovers an OLS bisector of $t_{\text{dep}} \propto \sigma^{-1.03 \pm 0.19}$. These different fitting methods, therefore, yield results that are within uncertainties of each other.

The error bars in Figure 2 are representative of the measurement uncertainties propagated through to the physical quantities. In the case of depletion time, however, it is likely that the systematic uncertainty is somewhat larger. The systematic uncertainty on t_{dep} could be as high as a factor of 2 for any single object (e.g., Bolatto et al. 2013). To determine the impact of this on the robustness of the correlation in Figure 2, we carry out a simple bootstrap experiment. We randomly modify the $\log(t_{\text{dep}})$ values to scatter around each point within a Gaussian distribution with $\sigma_{\text{Gauss}} = 0.15$ dex. We ran 1000 iterations, determining the correlation coefficient and p -value of each realization. We find that the median correlation coefficient is $r = -0.63$ with a standard deviation of 0.11 and the median $p = 0.006$ with a standard deviation of 0.04. We rerun this with the more pessimistic assumption of a

flat distribution with width of ± 0.15 dex and find a similar median correlation coefficient of $r = -0.6$ and a p -value still indicating a strong correlation, with median $p = 0.01$. Removing G20-2 from the fit reduces the robustness of the correlation, but with $r = -0.53$ and $p = 0.03$ the data still represent a high probability of correlation. Therefore, the correlation we observe in Figure 2 appears to be robust against the systematic uncertainties on the depletion time.

As we state above, exclusion of G20-2 in the fitted sample only marginally affects the robustness of the fit, measured by either Pearson's r or the p -value. Both sample choices satisfy definitions of "strong correlation" based on these statistical metrics. However, inclusion (or exclusion) of G20-2 does have a significant impact on the power law in the correlation between t_{dep} and σ . Future samples that contain more galaxies with $t_{\text{dep}} \lesssim 0.5$ Gyr would be helpful to further constrain the exact value of the power law. With our current sample there appears to be enough evidence to support a statistically significant inverse correlation between t_{dep} and σ , with the power law ranging between σ^{-1} and $\sigma^{-1.4}$. We will therefore consider predictions within this range consistent with our data set.

We note that the systematic observational effect of increased velocity dispersion on α_{CO} should result in the opposite trend. If the velocity dispersion of gas is increased by components other than internal cloud properties, then the effect is a systematic increase in observed CO luminosity (see discussion in Bolatto et al. 2013). This would increase the observed t_{dep} in galaxies with larger σ . Our observations of the opposite trend in Figure 2 then imply that this correlation is likely physical, and may even be steeper than our observations if we consider variations in α_{CO} .

Before we compare our observational results to predictions from theory, we point out an important assumption. Our measurement of velocity dispersion relies on ionized gas velocity dispersion maps, whereas theoretical predictions refer to total gas or molecular gas velocity dispersions. Ionized gas velocity dispersions include broadening due to thermal broadening. For a gas of 10^4 K this broadening amounts to $\sigma_{\text{br}} \approx 10 \text{ km s}^{-1}$ and is added in quadrature with the line width due to the motion of gas, such that the observed velocity dispersion is $\sigma_{\text{obs}}^2 \approx \sigma_{\text{gas}}^2 + \sigma_{\text{br}}^2$. For galaxy samples with lower measured velocity dispersions, such as in dwarf galaxies (as shown in Moiseev et al. 2015), this can be a significant contribution; however, our observed velocity dispersions range from 26 to 81 km s^{-1} . Thermal broadening will at most contribute $1\text{--}2 \text{ km s}^{-1}$.

Levy et al. (2018) find in nearby spiral galaxies that ionized gas gives systematically lower rotation velocities than molecular gas. They argue that in low- z spiral galaxies the molecular gas resides in a thin disk, where the ionized gas traces a thicker, more turbulent component. However, it is not clear whether the same result holds for galaxies, like DYNAMO and $z = 1\text{--}2$ main-sequence galaxies, that have significantly higher surface densities of gas and star formation. White et al. (2017) argue that for systems in dynamical equilibrium, which have large gas mass surface densities, the bulk of the gas will naturally have higher scale heights, which they show are well represented by the velocity dispersions measured with ionized gas in DYNAMO galaxies. Ultimately this field would significantly benefit from direct comparisons of ionized and molecular gas kinematics in gas-rich, turbulent

disks; such studies are at present sparse. Recent work by Übler et al. (2018) compares ionized gas and molecular gas kinematics in a single star-forming disk galaxy at $z = 1.4$. They find that the kinematics, both rotation and velocity dispersion, for the two tracers agree well, within $1\text{--}5 \text{ km s}^{-1}$. More work on this comparison would certainly be welcome; nonetheless, the evidence thus far seems to suggest that at high SFR and high σ_{ion} the ionized gas is a good tracer of the gas kinematics. We therefore make the same assumption as other studies (e.g., Förster Schreiber et al. 2009; Lehnert et al. 2009; Green et al. 2010; Genzel et al. 2011; Wisnioski et al. 2015; Krumholz & Burkhardt 2016) that for our sample $\sigma_{\text{ion}} \approx \sigma_{\text{gas}}$.

Theories of the interstellar medium (ISM) that incorporate feedback from star formation predict coupling of t_{dep} and σ that is similar to our observations (Ostriker et al. 2010; Shetty & Ostriker 2012; Faucher-Giguère et al. 2013; Krumholz et al. 2018). In all of these theoretical derivations it is shown that in the limit of marginal stability the turbulent velocity has a linear relationship with the star formation efficiency. If we assume that in our targets the ionized gas velocity dispersion is mostly driven by turbulence, then these models predict $t_{\text{dep}} \propto \sigma^{-1}$. This is represented as a dotted line in Figure 2 and is consistent with our data, assuming an arbitrary scale factor. In a subsequent section we will return to the topic of the scale factor in the $\sigma\text{--}t_{\text{dep}}$ correlation in light of results presented there.

Salim et al. (2015) derive a star formation law using a multi-freefall prescription of the gas (see also Federrath & Klessen 2012). They predict that star formation efficiencies will depend on both the probability density distribution and the sonic Mach number of the turbulence. In the limit that the virial parameter is not significantly variable, the Mach number is directly proportional to the velocity dispersion. These models then predict $t_{\text{dep}} \propto \sigma^{-4/3}$, which is shown as a dashed line in Figure 2. The prediction based on the multi-freefall model is almost exactly the same as our best-fit relation to our entire data set, $t_{\text{dep}} \propto \sigma^{-1.39}$.

In the comparison of both the theories of feedback-regulated star formation and the multi-freefall model one must consider the variation of the freefall time, t_{ff} . A relationship between σ and t_{dep} in star formation theory can be taken from Equation (20) of Shetty & Ostriker (2012), which states that $\sigma \propto (t_{\text{ff}}/t_{\text{dep}}) (p_*/m_*)$. Therefore, our interpretation of Figure 2 assumes that t_{ff} varies less than t_{dep} and σ . Similarly, with the results of Salim et al. (2015), the simple relationship $t_{\text{dep}} \propto \sigma^{-3/4}$ can only be derived by assuming that one can neglect variation in t_{ff} .

For the sample of galaxies in Figure 2 we expect that significant variation in the galaxy-averaged freefall time is unlikely. We expect that $t_{\text{ff}} \propto 1/\sqrt{\rho}$ (Krumholz & McKee 2005), where ρ is the volume density. We can estimate the variation in ρ using the parameters Σ_{gas}/h_z , where h_z is the gas scale height. For galaxies with longer $t_{\text{dep}} \sim 1\text{--}2 \text{ Gyr}$ the typical surface density in our sample is $10\text{--}50 M_{\odot} \text{ pc}^{-2}$. We surmise that these lower- σ galaxies likely have a disk thickness that is similar to the Milky Way, of order $\sim 100 \text{ pc}$. For a clumpy galaxy with lower t_{dep} and higher σ the gas surface density is typically $100\text{--}1000 M_{\odot} \text{ pc}^{-2}$. For these we assume a disk thickness that is similar to that of $z \sim 1$ edge-on galaxies, $500\text{--}1000 \text{ pc}$ (Elmegreen et al. 2005). Bassett et al. (2014) also present a discussion of two DYNAMO disk thicknesses based on kinematics of stars and gas; they conclude that h_z is in the

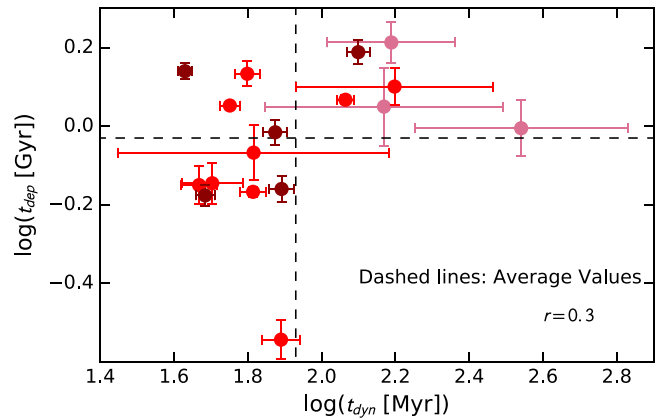


Figure 3. Relationship between galaxy depletion time and dynamical time. Symbol colors represent the source of data as described in Figure 1. The dashed lines indicate the averages for each quantity. We observe a very weak correlation ($r = -0.30$). The best fit is $t_{\text{dep}} \propto t_{\text{dyn}}^{0.44}$, with considerable scatter.

range of $400\text{--}1000 \text{ pc}$. Even though the galaxies in the lower left portion of Figure 2 have higher surface densities, they are also thicker, and therefore the value of $1/\sqrt{\Sigma_{\text{gas}}/h_z}$ will not change much across the sample in Figure 2. This is consistent with the results of Krumholz et al. (2012), who find that the distributions of freefall times of “high- z disks” and “ $z = 0$ spirals” overlap. Moreover, any variance in t_{ff} over this small dynamic range is likely to be significantly affected by stochastic scatter. However, if we extended our sample to either very lower surface density disks or perhaps very extreme starbursting disks at $z \sim 4$, this assumption that t_{ff} does not significantly vary may not be as valid. We note that there is significant uncertainty on the scale height of the molecular disk in gas-rich disk galaxies, and more work needs to be undertaken to study this important quantity. We also note that these are galaxy-averaged quantities. It is very likely that measurements at the scale of individual molecular clouds have increased scatter and perhaps a different parameter dependency due to the more significant variation of the freefall time.

3.2. Dynamical Time

A number of theories and semianalytic models suggest that the gas depletion time should be directly connected to the dynamical time, $t_{\text{dyn}} = 2\pi R_{\text{disk}}/V_{\text{flat}}$, of the galaxy (e.g., Davé et al. 2011; Krumholz et al. 2012). These models are motivated by the well-known relationship $\Sigma_{\text{SFR}} \propto \Sigma_{\text{gas}}/t_{\text{dyn}}$ observed in nearby galaxies (Kennicutt 1998). Krumholz et al. (2012) argue that in the “Toomre regime,” in which galaxies have high gas fractions and show marginal stability, the local star-forming region is not able to decouple from the ambient gas in the galaxy. From this concept they then derive a positive, linear correlation between t_{dyn} and t_{dep} .

In Figure 3 we show the relationship between depletion time and galaxy dynamical time for galaxies in our sample. The depletion time does have some dependency on t_{dyn} in that galaxies with $t_{\text{dep}} \lesssim 1 \text{ Gyr}$ always have low t_{dyn} . An effort to fit a correlation returns a very weak, high-scatter relationship, with a Pearson’s correlation coefficient of $r = 0.3$ and a p -value for this data set of 0.2. The best-fit relationship for our data set is

$$\log(t_{\text{dep}}) = 0.44 \pm 0.24 \log(t_{\text{dyn}}) - 0.44 \pm 0.23. \quad (4)$$

This is significantly shallower than the prediction for gravity-driven turbulence (Krumholz et al. 2012). We find no correlation at all between t_{dep} and the product of $Q \times t_{\text{dyn}}$, which is also predicted in the gravity-only theory. We find that using the same bootstrap method as used to analyze Figure 2, to account for systematic uncertainty in t_{dep} , results in a median correlation coefficient of $r = 0.25$ with a standard deviation of 0.16, and the median p -value is 0.3. These values indicate a very low probability of a correlation between t_{dep} and t_{dyn} in our data set.

4. Effect of Extreme Pressure on Star Formation in Turbulent Disks

Motivated by the qualitative success of feedback-regulated star formation models in describing the relationship between t_{dep} and σ , we now consider a fundamental prediction of those same models, the relationship between Σ_{SFR} and midplane hydrostatic pressure, P . Theories describing the formation of compact star clusters in very high pressures have been in development for some time (Elmegreen 1989; Elmegreen & Efremov 1997), and observations of gas-rich, star-forming disk galaxies suggest that pressures can become very high compared to low- z spirals (Swinbank et al. 2011).

It is proposed in a number of models that star formation in disk galaxies is a self-regulating process, in which the pressure of the system is balanced by the feedback processes associated with star formation (e.g., Ostriker & Shetty 2011; Shetty & Ostriker 2012; Kim et al. 2013). The semianalytic models in Ostriker & Shetty (2011) predict a linear relationship between pressure and Σ_{SFR} , and the simulations of Kim et al. (2013) find a nearly linear relationship.

4.1. Estimating the Total Midplane Pressure

In this work we use the following formula from Elmegreen (1989) to estimate the midplane hydrostatic pressure within our galaxies:

$$P = \frac{\pi}{2} G \Sigma_g \left[\Sigma_g + \left(\frac{\sigma}{\sigma_*} \right) \Sigma_* \right]. \quad (5)$$

Σ_{gas} and Σ_* represent the gas and stellar mass surface densities, and similarly σ and σ_* represent velocity dispersions of the gas and stars.

In Appendix B we outline our method to measure or estimate each of these parameters described in Equation (5), as well as discuss in detail the impact of the uncertainty in each parameter on the pressure. We briefly summarize our main sources of uncertainty here. We also note that Equation (5) was originally developed to describe subgalactic measurements of the ISM. Our use of it here requires the assumption that the ensemble averages of the galaxy are reflective of local values, though systematic biases may exist.

The largest source of uncertainty in pressure comes from our use of unresolved CO flux measurements. To calculate Σ_{gas} , we assume that the size of the ionized gas disk is equivalent to the size of the molecular gas disk. This assumption is consistent with observations of high- z galaxies (Tacconi et al. 2013; Bolatto et al. 2015; Dessauges-Zavadsky et al. 2015; Hodge et al. 2015) with an uncertainty of 20%–50%. However, we also consider the possibility that the molecular disk is as large as our unresolved CO measurement. This reduces the

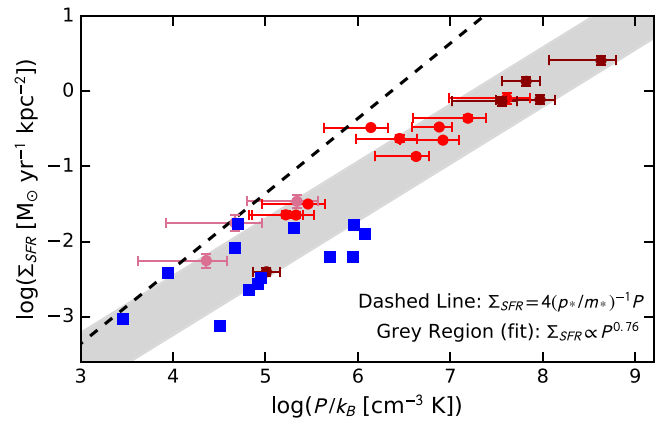


Figure 4. Comparison of SFR surface density to midplane hydrostatic pressure. The DYNAMO galaxies are labeled according to data source as described in Figure 1. In this figure we also include measurements from Leroy et al. (2008) using THINGS data. The dashed line represents the theoretical prediction. We find a strong, sublinear relationship spanning 4–5 orders of magnitude in both Σ_{SFR} and pressure.

pressure by a factor of ~ 4 in most targets and is reflected in the error bars of Figure 4. We also consider the uncertainty introduced from different assumptions of the atomic hydrogen surface density. We find that this only has a significant impact on the two lowest-pressure systems and is likewise reflected in the error bars. For more information on these uncertainties see Appendix B.

To increase sampling at low pressures, we combine our sample set here with the observations of the THINGS sample (Walter et al. 2008), using derived measurements from Leroy et al. (2008) to calculate Σ_{SFR} and P . The combined data set spans nearly 6 orders of magnitude in midplane pressure and 4 orders of magnitude in Σ_{SFR} . We note that there are important differences between the THINGS and DYNAMO measurements of pressure. The THINGS sample has measured values of both molecular and atomic gas mass surface density, where the DYNAMO sample only has observations of molecular gas mass and atomic gas mass surface density is adopted. This is likely important at lower pressure, where the ratio of molecular to atomic gas mass surface density is lower. Alternatively, THINGS galaxies do not have measurements of ionized gas velocity dispersions. Leroy et al. (2008) adopt $\sigma \approx 11 \text{ km s}^{-1}$ as being consistent with their measurements of atomic gas. These considerations are discussed in more detail in Appendix B. We have five DYNAMO galaxies that overlap the range in derived pressure and Σ_{SFR} with those of the THINGS galaxies. We find the two samples to have similar values of Σ_{SFR}/P .

For DYNAMO galaxies we find very high values of P/k_B compared to local spirals like the Milky Way, reaching as much as 10^5 times higher than the pressure in the Milky Way. This is similar to the pressure of the $z \sim 2$ galaxy observed in Swinbank et al. (2011). DYNAMO galaxies have both significantly higher gas masses and smaller sizes compared to Milky-Way-like spirals. These differences lead to greater surface densities, which then create very high pressures that we observe. In almost all galaxies the “stellar term” of the pressure, $(\sigma/\sigma_*)\Sigma_*$, dominates over the “gas term,” Σ_g . This is notable, as the gas fractions of DYNAMO galaxies are very high, $f_{\text{gas}} \sim 20\%$ – 60% . Even in this sample of gas-rich galaxies we find that on average $P_{\text{star}}/P_{\text{gas}} \approx 2.3 \pm 1.1$. We note that this is a prediction of feedback-regulated star

formation, and that even in gas-rich systems the stars contribute a very important component to the pressure (Ostriker & Shetty 2011). We will return to this subject in our discussion of dynamical equilibrium pressure.

4.2. Balance of Star Formation and Pressure in Gas-rich Disks

In Figure 4 we compare the midplane hydrostatic pressure P , as described in Equation (5), with the SFR surface density. We find that a single correlation describes these data well, over 6 orders of magnitude in pressure. The best-fit relation is

$$\log(\Sigma_{\text{SFR}}) = (0.76 \pm 0.06)\log(P/k_B) - 5.89 \pm 0.35, \quad (6)$$

where Σ_{SFR} is in units of $M_{\odot} \text{ yr}^{-1} \text{ kpc}^{-2}$ and P/k_B is in units of $\text{cm}^{-3} \text{ K}$. The 1σ vertical scatter around this relationship is represented as the shaded gray region in Figure 4.

It is predicted that $\Sigma_{\text{SFR}} = 4(p_*/m_*)^{-1} P_{\text{tot}}^N$, where the power-law index N is expected to be close to unity (e.g., Shetty & Ostriker 2012; Kim et al. 2013). Our correlation in Figure 4 is then qualitatively consistent with the prediction of a strong, positive relationship between these two quantities.

The power-law slope we observe in Figure 4 is significantly below unity, which is different from the predictions described above (shown as the dashed line in the figure). In simulations by Kim et al. (2013) the measured power law is slightly steeper than linear. In a subsequent section of this paper we discuss three possible options to explain this discrepancy: (1) that the relationship between pressure and Σ_{SFR} is truly nonlinear; (2) that the scale factor p_*/m_* is nonuniversal and increases for gas-rich, high-pressure disks; and/or (3) that alternate mechanisms, such as mass transport within a disk, also provide pressure support.

It is important to note that both systematic and observational uncertainties in the calculation of P/k and Σ_{SFR} can affect these results at the factor of a few level. For example, to calculate mass surface density, we estimate the size of the disk as $R_{\text{disk}} = 2 R_{1/2}$. However, since pressure scales as mass surface density squared, adopting a different characteristic radius of the galaxy would alter pressure more than Σ_{SFR} . The median value for these low-pressure systems is $P/\Sigma_{\text{SFR}} \approx 9 \times 10^3 \text{ km s}^{-1}$, which is only a factor of a few higher than the theoretical prediction, and as shown in Figure 4, the predicted value falls within the scatter of low-pressure systems. Considering this, we therefore conclude that for disks with lower values of pressure ($P/k < 10^6 \text{ cm}^{-3} \text{ K}$) the data are within the uncertainty of the predictions from the models. This is to say that our data suggest that local universe spirals are consistent with theoretical predictions of $\Sigma_{\text{SFR}}-P$ from feedback-regulated star formation models. This is similar to the results of Herrera-Camus et al. (2017), who find that KINGFISH galaxies, with $P/k \sim 10^3.5-10^4.5$, are consistent with predictions from Kim et al. (2013).

High-pressure systems, $P/k > 10^6 \text{ cm}^{-3} \text{ K}$, however, do not appear to be reconcilable with even generous estimations of the uncertainties. If we consider only those systems with $P/k > 10^6 \text{ cm}^{-3} \text{ K}$, we find an average value of $\langle P/\Sigma_{\text{SFR}} \rangle \approx 4.4 \times 10^4 \text{ km s}^{-1}$. This is more than an order of magnitude larger than the theoretical prediction, as shown in Figure 4.

In light of these high values of P/Σ_{SFR} in DYNAMO galaxies, we now consider the zero-point in Figure 2. We can compare the scale factor in Figure 2 to that of Figure 4 by

solving each theoretical prediction for p_*/m_* . Shetty & Ostriker (2012) predict that $\sigma \approx 0.366 (t_{\text{ff}}/t_{\text{dep}}) (p_*/m_*)$, where t_{ff} is the freefall time. Note that this is adopted from Equation (20) of Shetty & Ostriker (2012). The estimate using t_{dep} and σ does not require all of the assumptions that go into measurement of galaxy pressure (described in detail in Appendix B); most notably, galaxy sizes are not used in this case. However, this derivation depends on an assumption of the freefall time, which introduces a source of uncertainty. Nonetheless, we can think of this method of deriving the scale factor as a semi-independent check. The freefall time of a cloud will depend on the inverse square root of the local gas density (Krumholz et al. 2012). For a gas-rich, turbulent disk Krumholz et al. (2012) suggest values of $t_{\text{ff}} \approx 1-10 \text{ Myr}$. Using this range, we derive values of $p_*/m_* \approx 10^4-10^6 \text{ km s}^{-1}$ for DYNAMO galaxies, which is consistent with our estimate from P/Σ_{SFR} . We find that there is a high-scatter correlation, and on average, the values of p_*/m_* derived from the two methods are in agreement.

We caution that it is not necessarily the case that P/Σ_{SFR} is a unique, robust tracer of the true physical balance of these quantities over the entire range of galaxies. That is to say, systematic uncertainties could affect this correlation at some level. Most notably, the CO-to- H_2 conversion factor could be a function of pressure (Narayanan et al. 2011).

4.3. Dynamical Equilibrium Pressure

We also consider the ‘‘dynamical equilibrium pressure’’ as described in Kim et al. (2011),

$$P_{\text{DE}} \approx \frac{\pi G \Sigma_g^2}{2} + \Sigma_g (2G \rho_{\text{SD}})^{1/2} \sigma, \quad (7)$$

where ρ_{SD} is the total midplane density, including dark matter and stars, as defined in Ostriker & Shetty (2011). The total midplane density $\rho_{\text{SD}} = \Sigma_*/h_z + (V_{\text{flat}}/R_{\text{disk}})^2/(4\pi G)$. The quantity h_z is the disk thickness; we describe how we calculate it in Appendix B. As described before, we make the simplifying assumption that in galaxies with high gas velocity dispersion, like the DYNAMO sample, the velocity dispersion measured from ionized gas is a good representation of σ for the total gas. The dynamical equilibrium pressure is an alternate description of the pressure, under the assumption that the system has evolved to its equilibrium state, in which pressure balances the feedback mechanism.

An interesting feature of representing pressure as done in Equation (7) is that this directly ties the result in Figure 2 to the effect of increasing pressure. We note again that this is under the assumption that $\sigma_z \approx \sigma_{\text{los}}$. If vertical dynamical equilibrium in a disk is satisfied, then Ostriker et al. (2010) predict that $P \propto \Sigma \sqrt{\rho_{\text{SD}}}$ and also, as discussed above, $\Sigma_{\text{SFR}} \propto P_{\text{DE}}$. Therefore, in order for a linear (or nearly linear) relationship between pressure and also $t_{\text{dep}} \propto 1/\sigma$ to hold, the stellar gravity term ($\sigma \sqrt{2G \rho_{\text{SD}}}$) from Equation (7) must dominate over the gas gravity term ($\pi G \Sigma/2$). Therefore, a direct prediction of the feedback-regulated theory of star formation in starbursting disk galaxies, which we can test with our data, is that $\pi G \Sigma/2 < \sigma \sqrt{2G \rho_{\text{SD}}}$. We find that for all galaxies in the DYNAMO sample the stellar gravity term dominates over the gas term. We find that on average the ratio of star to gas terms is ~ 7 . The lowest values of star to gas terms are in

systems with, as one would expect, larger gas fractions, $M_{\text{mol}}/M_{\text{dyn}} \sim 30\%–80\%$; however, the ratio remains above 1, reaching down to as low as ~ 3 for galaxies in our sample.

5. Discussion of Results

5.1. Inverse Correlation of t_{dep} and σ

In Figure 2 we show a strong correlation ($r \approx -0.8$ and $p\text{-value} = 10^{-4}$) between the molecular gas depletion time and velocity dispersion of the ionized gas, such that $t_{\text{dep}} \propto \sigma^{-1.39 \pm 0.23}$. We have tested this correlation against the systematic uncertainties introduced from the scaling of ionized gas emission lines to SFRs, as well as converting CO (1–0) line flux to molecular gas mass. We find the correlation in our sample to be robust. Indeed, we find that t_{dep} correlates more strongly with σ than any other parameter we compared it to (e.g., SFR/M , Σ_{SFR} , t_{dyn} , Σ_{star}).

The inverse correlation between t_{dep} and σ seems inconsistent with predictions in which the turbulence is driven only by gravity, which do not incorporate more complex treatments of turbulence (e.g., Federrath & Klessen 2012). Krumholz et al. (2012), in their Equation (18), determine that for a system in which the turbulence is driven exclusively by gravity $t_{\text{dep}} \propto Q t_{\text{dyn}}$, where Q is Toomre’s stability parameter and t_{dyn} is the dynamical time of the galaxy. The depletion time of marginally stable disks, such as our sample, is therefore predicted to mostly be driven by the dynamical time; however, our data set does not support a strong correlation between t_{dyn} and t_{dep} . We note the caveat that although there is very little evidence to support a galaxy-averaged relationship between t_{dep} and t_{dyn} , Krumholz et al. (2012) suggest that a local relationship may be stronger (where t_{dep} and t_{dyn} are measured in radial bins). This is not possible to measure with our current data set; resolved observations of CO in turbulent disks would be very helpful to this end.

Theories in which turbulence is driven by feedback (e.g., Ostriker & Shetty 2011; Shetty & Ostriker 2012; Faucher-Giguère et al. 2013), however, predict an inverse relationship $t_{\text{dep}} \propto \sigma^{-1}$. As we show in Figure 2, this power-law slope is consistent with our observations.

Using a multi-freefall timescale prescription for the gas also agrees with our results (Federrath & Klessen 2012; Salim et al. 2015). The critical parameters in these models include the probability density function and sonic Mach number of the gas. These models are not necessarily inconsistent with feedback-driven models, in that feedback could still drive the compressive form of turbulence, which then produces a different distribution of freefall times.

5.1.1. Possible Implications for Cosmic Evolution of t_{dep}

The results we find in this paper may shed some light on the observed shallow evolution of depletion time with redshift (Genzel et al. 2015; Schinnerer et al. 2016; Scoville et al. 2016; Tacconi et al. 2017). Theories that drive gas depletion time via the cosmic evolution of the dynamical time predict an order-of-magnitude decrease in t_{dep} . However, recent observations of high-redshift galaxies find that depletion times drop by a factor of 2–5 from $z = 0$ to $z = 4$. As we have discussed above in the theory of feedback-regulated star formation, a lower gas depletion time is natural in systems that have both high pressure and high internal velocity dispersion.

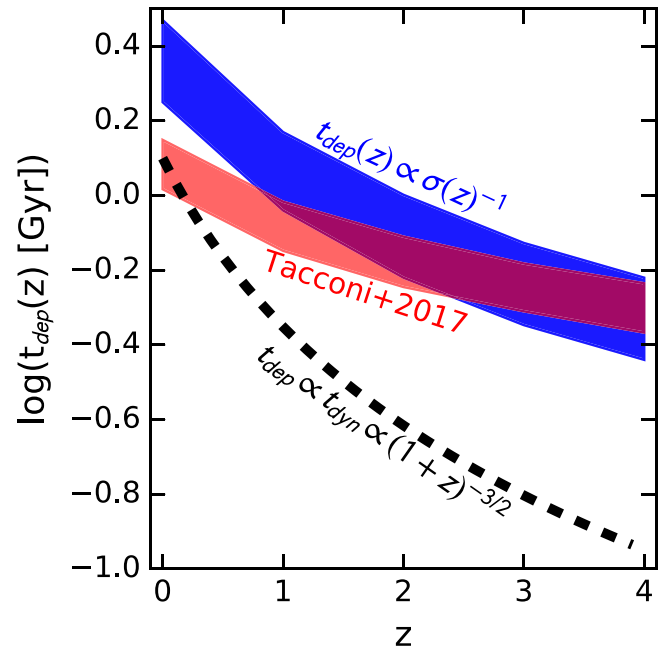


Figure 5. Consideration of the very simple toy model in which the redshift evolution of the depletion time is a function of the cosmic evolution of the velocity dispersion. The blue shaded region represents depletion times as determined from a σ^{-1} dependency, similar to that found in Figure 2. The values of $\sigma(z)$ are taken from Wisnioski et al. (2015). The dashed line represents the expected evolution if t_{dep} is determined only by the dynamical time. The red shaded region represents the cosmic evolution of depletion time from the composite data set of Tacconi et al. (2017). This simple model is a good match to observations at $z > 1$.

In Figure 5 we compare the observed cosmic evolution of molecular gas depletion time to the prediction based on a simple model using a $t_{\text{dep}} \propto \sigma^{-1}$ dependency set to match our observations in Figure 2. Wisnioski et al. (2015) present the gas velocity dispersion, from emission lines, over a range in redshift $z \sim 0–3.5$. We use the average cosmic evolution of σ (z), from Wisnioski et al. (2015), to determine $t_{\text{dep}}(\sigma)$ as a function of redshift. The observed cosmic evolution of t_{dep} is from the empirical fit to the main-sequence evolution of the composite data set of Tacconi et al. (2017). The predicted values of t_{dep} agree with observations for $z > 1$. This implies first that our results likely hold on high- z galaxies, at least in a bulk sense. Moreover, this may imply that star formation efficiencies at high redshift are regulated not only by the availability of gas but also by the feedback within the disk.

At $z \sim 0$ our simple model overpredicts the data by a factor of 2–3. This is not at all surprising. Many of the assumptions that go into our analysis are not valid for low- z spirals. (We remind the reader that DYNAMO galaxies are atypical galaxies for the low- z universe.) First, unlike our galaxies, the velocity dispersion for typical low- z spirals is quite low ($\sigma < 20 \text{ km s}^{-1}$). As we discuss above, ionized gas measurements are more significantly affected by thermal broadening at low dispersion, and ionized gas in more typical, low-SFR, low- z spirals may overestimate the true gas velocity dispersion. Also, at $z \sim 0$ the gas almost certainly becomes far more dominated by the atomic component than in $z > 1$ galaxies (Obreschkow & Rawlings 2009).

In Figure 5 we also show the expected evolution of the depletion time if it were exclusively a function of the dynamical time, $t_{\text{dep}} \propto t_{\text{dyn}} \propto (1+z)^{-3/2}$ (see arguments in

Davé et al. 2011; Krumholz & Burkhardt 2016). This predicts significantly more evolution than in observations. Similarly, Lagos et al. (2015) predict a very steep evolution to the depletion time. We interpret this to imply that internal processes, such as the regulation of star formation via feedback, are therefore a dominant factor in determining the evolution of the depletion time over the past ~ 10 billion years.

5.2. Implications of $\Sigma_{\text{SFR}}-P$ Correlation

We find that in our data set Σ_{SFR} and the midplane pressure of galaxies have a very tight correlation across almost 6 orders of magnitude in pressure using two different formulations of midplane pressure (Figure 4). These correlations are found to be sublinear with $\Sigma_{\text{SFR}} \propto P^{0.77}$. Our measurements are therefore not as steep as theories that predict $\Sigma_{\text{SFR}} \propto P$ (Ostriker et al. 2010; Kim et al. 2011).

There appear to be three possibilities to reconcile our observations with the theoretical predictions: (1) the relationship between SFR surface density and pressure is sublinear, (2) the feedback momentum injected into the ISM per unit new stars formed (p_*/m_*) changes as a function of the local ISM properties, and/or (3) alternate mechanisms could drive turbulence and provide support against gravitational pressure.

From our data alone we cannot uniquely distinguish between these scenarios. We will consider these options below. We note to the reader that there is also the possibility that each of these options is contributing to the offsets we observe.

5.2.1. Is Σ_{SFR} versus P Truly Nonlinear?

Benincasa et al. (2016) simulate feedback-regulated star formation and qualitatively report a sublinear relationship between Σ_{SFR} and pressure. They argue that feedback affects the scale height of the disk nonlinearly, which affects the pressure and gives rise to this sublinearity. Benincasa et al. (2016) do not estimate an actual value for the power law. Hence, we cannot quantitatively determine whether this effect matches our data. If so, then one could assume that the normalization in our Equation (6) can be used to estimate the feedback momentum, $p_*/m_* \approx 2700 \text{ km s}^{-1}$. This is similar to the commonly adopted value. Quantitative analysis of the $\Sigma_{\text{SFR}}-P$ relationship in 3D simulations would therefore be informative.

Observational effects could possibly contribute to a nonlinearity as well between Σ_{SFR} and P . Narayanan et al. (2012) argue from simulations that the CO-to-H₂ conversion factor may be lower in regions of higher molecular gas surface density. We note that over the range of normal spirals empirical studies of the CO-to-H₂ conversion factor do not find significant variation with gas mass surface density (Sandstrom et al. 2013). Bolatto et al. (2013) argue that the baryonic surface density could decrease α_{CO} , but this would only be at the $\sim 50\%$ level. It would not fully reconcile our most extreme observations in Figures 4 with the theoretical prediction. Moreover, global studies of $z = 1-2$ main-sequence galaxies find that the standard Milky Way conversion factor is consistent with dust mass estimates (Genzel et al. 2015; Tacconi et al. 2017). White et al. (2017) find similar results with DYNAMO galaxies.

5.2.2. Does p_*/m_* Vary from Local Spirals to High-pressure Turbulent Disks?

In theoretical predictions the scale factor in the relationship between pressure and SFR surface density is directly proportional to the momentum feedback per stellar mass, p_*/m_* . In the case that feedback is generated by supernovae, this quantity, p_*/m_* , represents the momentum injected into the ISM from supernovae per unit stellar mass of new stars formed. It is therefore a critical parameter in models of feedback-regulated star formation. Most theories of feedback-regulated star formation use an adopted or calculated value of $p_*/m_* \sim 3000 \text{ km s}^{-1}$ (e.g., Ostriker & Shetty 2011; Shetty & Ostriker 2012; Faucher-Giguère et al. 2013; Kim et al. 2017). The dashed line in Figure 4 is set to represent the theoretical prediction.

The nonlinearity in Figure 4 could be driven by changing values of p_*/m_* across the range of pressures. If this is the case, our data would be consistent with local spirals, such as THINGS galaxies, having values of p_*/m_* that are roughly consistent with theoretical predictions, but higher-pressure systems have significantly higher values of momentum injection.

We also derive similarly high values of p_*/m_* in DYNAMO galaxies from the $t_{\text{dep}}-\sigma$ correlation in Figure 2, which at face value provides a semi-independent line of evidence that p_*/m_* is changing. Krumholz & Burkhardt (2016) and Krumholz et al. (2018) have likewise noted that feedback-only models of the ISM have trouble reproducing the large velocity dispersions observed in $z \sim 2$ turbulent disk galaxies.

The universality of p_*/m_* is currently under some debate. Some recent simulations suggest that clustering of supernovae could increase the momentum input per star formation by factors of ~ 10 (Gentry et al. 2017). Conversely, Kim et al. (2017) find that the injected momentum per mass of star formation would not be significantly higher in environments with higher number density of supernovae. More recent simulations from Gentry et al. (2019) that model feedback in a 3D, magnetized medium argue that previous results may be due to numerical effects.

We note that in the highest-pressure systems $p_*/m_* = 4P/\Sigma_{\text{SFR}} \approx 10^5 \text{ km s}^{-1}$, which is higher than even the most extreme predictions (Gentry et al. 2017). This may indicate that varying p_*/m_* alone is not able to account for the discrepancy with our data. Resolved observations of Σ_{SFR} and P in galaxies like DYNAMO would be useful to further understand the range of values of P/Σ_{SFR} .

5.2.3. Are Alternate Sources of Pressure Support Important in Gas-rich Disks?

The models we consider above assume that feedback is primarily driven by supernovae. Physical models that include higher amounts of radiation feedback, for example, larger rates of momentum injection due to the inclusion of radiation pressure, photoionization, and winds (e.g., Hopkins et al. 2011, 2014; Murray et al. 2011), are able to generate larger velocity dispersions than those that assume that feedback is dominated by supernovae, such as Ostriker & Shetty (2011). This too remains under debate; high-resolution, detailed simulations of molecular clouds (Kim et al. 2018) suggest that the contribution that radiation feedback makes to p_*/m_* would be quite small ($10^1-10^2 \text{ km s}^{-1}$) compared to supernovae. Moreover,

radiation feedback is found to be even less important in high surface density molecular clouds, which the DYNAMO galaxies would likely contain.

Recently, Krumholz et al. (2018) present a model in which pressure support comes from both mass transport and feedback. Similar to Krumholz & Burkhardt (2016), they predict a linear relationship between σ and SFR that matches data, including DYNAMO galaxies, with significant scatter. It is possible that in galaxies with higher gas mass surface densities, and hence higher pressures, mass transport plays a more important role. It seems plausible that those galaxies with larger gas fractions would both have more available gas and likely be experiencing more active accretion, which could drive more turbulence. However, it is not clear how the relationship between t_{dep} and σ would in general be affected by such sources of pressure support. In the specific case that energy lost due to turbulent dissipation is equal to energy injected for supernovae, Krumholz et al. (2018) find, similar to Ostriker et al. (2010), that $t_{\text{dep}} \propto \sigma^{-1}$, which is consistent with our main result in Figure 2. It is not clear what values of P/Σ_{SFR} would exist in this mixed model, nor in those including other forms of feedback, e.g., radiation pressure.

6. Summary

Overall our results show qualitative agreement with a number of predictions in feedback-regulated star formation models (e.g., Ostriker & Shetty 2011). These include (1) an inverse correlation between molecular gas depletion time and gas velocity dispersion; (2) a strong, positive correlation between SFR surface density and hydrostatic midplane pressure (as well as dynamical equilibrium pressure); and (3) that the contribution of stars to the pressure dominates over the gas, even in very gas-rich ($f_{\text{gas}} > 50\%$) galaxies.

We, however, find significant differences in the quantitative details of both the $t_{\text{dep}}-\sigma$ correlation and the Σ_{SFR} versus pressure correlations. From our data alone we cannot determine whether these correlations imply that (a) the true correlation between Σ_{SFR} and pressure is nonlinear or (b) the momentum injected into the ISM by star formation feedback (p_*/m_*) varies from low values in local spirals to very efficient values in high- z turbulent disks. Moreover, higher spatial resolution observations of molecular gas would help reduce the uncertainty on pressure. There is evidence from simulations that one or possibly both of these options may be contributing to the discrepancies between our observations and theory.

We have also shown that the predictions of feedback-regulated star formation, if modified to scale similar to DYNAMO galaxies, are able to account for the cosmic evolution of molecular gas depletion time. Going forward, comprehensive studies of both kinematics and gas mass will be useful for determining how relationships like that in Figure 2 hold in high-redshift galaxies. For example, at a given redshift does one see both an increase in σ and a decrease in t_{dep} in the same way as galaxies extend above the main sequence? We cannot test this with DYNAMO. Of course, high-quality data that can robustly control for galaxy morphology, etc., are currently difficult to obtain. Also, we note in closing that more exotic possibilities such as a top-heavy initial mass function in a high- Σ_{SFR} environment (e.g., Nanayakkara et al. 2017) could reduce SFR and thus flatten out the redshift evolution of t_{dep} ; more work to investigate this possibility could be informative. Finally, as stated above, maps of gas in turbulent disk galaxies

will be crucial to determine how pressure may be impacting the properties of massive star-forming clusters (as described in Elmegreen & Efremov 1997).

We are thankful to Cinthya Herrera for help in reducing NOEMA data. We are very grateful to Eve Ostriker, James Wadsley, and Christoph Federrath for helpful discussions while preparing this manuscript. D.B.F. is thankful to Sarah Busch for technical help. D.B.F., K.G., and S.S. acknowledge support from Australian Research Council (ARC) Discovery Program (DP) grant DP130101460. D.B.F. acknowledges support from ARC Future Fellowship FT170100376. A.D.B. acknowledges partial support from AST1412419. Some of the data presented herein were obtained at the W. M. Keck Observatory, which is operated as a scientific partnership among the California Institute of Technology, the University of California, and the National Aeronautics and Space Administration. The Observatory was made possible by the generous financial support of the W. M. Keck Foundation. This work is based on observations carried out with the IRAM Plateau de Bure Interferometer. IRAM is supported by INSU/CNRS (France), MPG (Germany), and IGN (Spain).

Appendix A

CO Spectra and Observational Details

In Table 3 we list the observation parameters and derived fluxes for CO (1–0) observations of DYNAMO galaxies. The observations were carried out in three separate campaigns with the PdBI, also called NOEMA. All observations were made with the WIDEX system. Each observing campaign had similar sensitivity goals of ~ 1.5 mJy in 50 km s^{-1} channels. Of the CO measurements used in this paper, eight have been published in previous works (Fisher et al. 2014; White et al. 2017). Details of those corresponding observations are also outlined in those papers.

Spectra of new observations are shown in Figure 6. Similar spectra for previously published observations are given in the respective publications. For each new observation we plot the flux density in mJy against the velocity in km s^{-1} . The redshifted CO (1–0) transition is centered at the velocity of 0 km s^{-1} . All fluxes are determined by binning the spectra into 50 km s^{-1} channels, as described in the methods section.

Appendix B

Estimation of Physical Parameters for Measurement of Pressure

B.1. Galaxy Sizes

The size of the starlight is measured from the continuum observations corresponding to each emission-line measurement. Similarly, the sizes used to calculate the SFR surface density are measured from the resolved emission-line maps for each target. For THINGS galaxies Leroy et al. (2008) measure the sizes in stars, SFR, and molecular gas, and for those targets we use the corresponding measurement to directly measure the associated surface brightness. Our observations of CO (1–0) in most DYNAMO targets are unresolved source detections, with a handful that are marginally resolved, in which R_{disk} is only slightly larger than the beam size. To calculate the total midplane pressure for DYNAMO galaxies, we therefore must make an assumption on the sizes of the molecular gas.

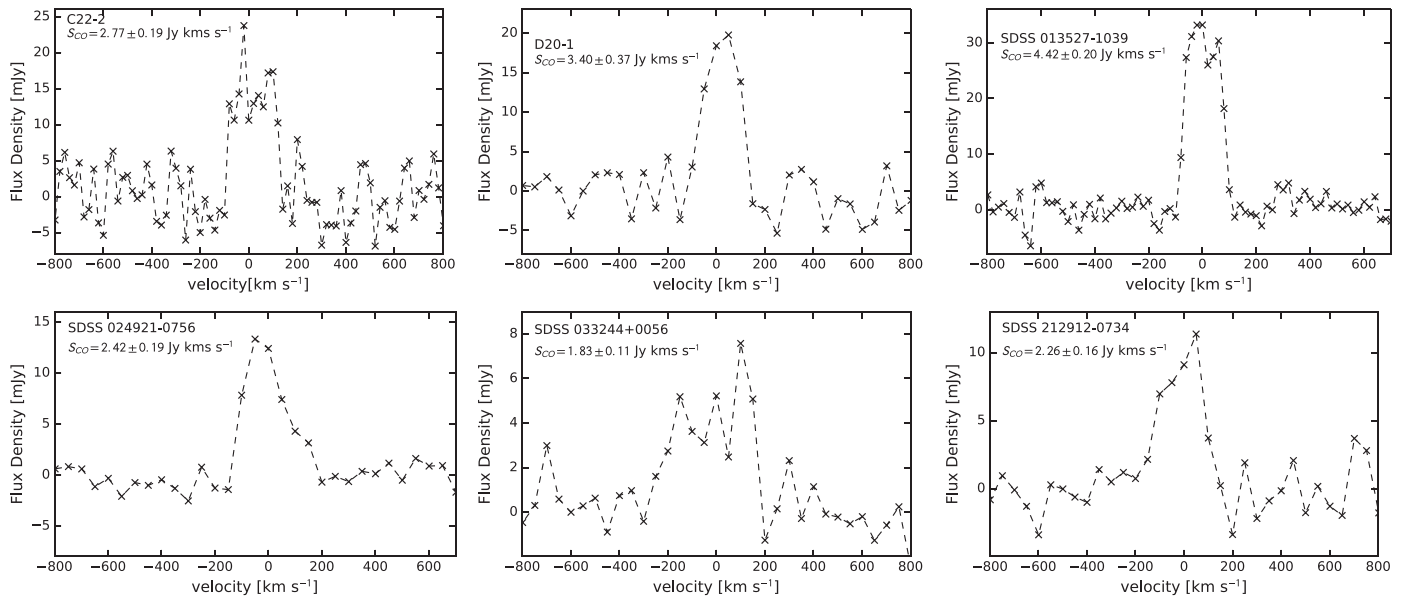


Figure 6. Above spectra represent data for new NOEMA observations used in this work. Each spectrum is centered on the redshifted CO (1–0) emission line. All flux densities are measured using a binning of 50 km s^{-1} .

A straightforward method to estimate the molecular gas disk is to assume that the half-light radius of the ionized gas is roughly equivalent to that of the molecular gas. In the local universe the surface brightness profiles of gas in disk galaxies have been shown to be well behaved with a regular, exponential decay (Bigiel & Blitz 2012). In the THINGS sample Leroy et al. (2008) find that the average ratio of CO to SFR scale lengths is $\langle l_{\text{CO}}/l_{\text{SFR}} \rangle = 1.0 \pm 0.2$. Assuming that the distribution of ionized gas is a good proxy for the distribution of the star formation, the assumption that $R_{1/2}(\text{CO}) \approx R_{1/2}(\text{H}\alpha)$ would be well justified in similar galaxies.

Due to the difficulties of such observations, there is considerably less work comparing the distribution of molecular gas to the distribution of stars, or star formation in turbulent disks. Hodge et al. (2015) measure the size of gas, CO (2–1), and star formation, $880 \mu\text{m}$, in a rare double-lensed system at $z \sim 4$ with $\sim 1 \text{ kpc}$ resolution, finding that the respective physical size of the disk is 14 kpc in CO and $\sim 10 \text{ kpc}$ in star formation. Bolatto et al. (2015) study high-resolution maps of CO (1–0) and CO (3–2) in two $z \sim 2$ targets, finding that the CO gas in these targets $R_{1/2}(\text{CO}) - R_{1/2}(\text{optical}) \approx 1 \text{ kpc}$. Similarly, the sample of Tacconi et al. (2013), which has considerably lower spatial resolution, nonetheless shows that on average $R_{1/2}(\text{CO})/R_{1/2}(\text{optical}) \approx 1$ with a standard deviation of 0.5. Dessauges-Zavadsky et al. (2015) map CO (2–1) in a sample of strongly lensed galaxies at $z \sim 2$ and find $R_{1/2}(\text{CO}) \sim 1\text{--}4 \text{ kpc}$, which is similar to our estimates from H α . We note that more extreme differences have been observed; however, those targets are typically found to have multiple velocity components, indicating that they are likely ongoing mergers (e.g., Spilker et al. 2016). Overall, the observations of main-sequence galaxies at $z > 1$ seem to suggest that the uncertainty on our estimation of $R_{1/2}(\text{CO}) \approx R_{1/2}(\text{H}\alpha)$ would be at the $\sim 20\%$ – 50% level. Increasing the size of the molecular gas disk by 50% (i.e., $R = 1.5 R_{1/2}(\text{H}\alpha)$) would decrease our measured pressures by a factor of 2–3 in DYNAMO galaxies.

For our unresolved observations we can use the measured beam size as an estimate of the “largest possible size” for the molecular gas disk in DYNAMO galaxies, which will then correspond to a lowest possible pressure. For the five galaxies in which the beam is slightly smaller than R_{disk} we use the radius at which the flux from the galaxy is equivalent to the noise. The median largest circularized radius of CO disk in the DYNAMO is ~ 1.6 times larger than the corresponding R_{disk} measured from the ionized gas. This corresponds to a decrease in the measured midplane pressure by a factor of 3–4.

The THINGS observations suggest that for normal spirals, low-pressure disks, assuming that the molecular gas and star formation have similar disk sizes, are safe approximations. Observations of higher-redshift sources suggest that this is roughly a safe assumption, though molecular disks in these higher-pressure systems may be slightly larger. We opt for the simple assumption that $R_{\text{disk}}(\text{CO}) \approx R_{\text{disk}}(\text{ion})$, as this is consistent with the data and allows us to make a single correction for low- and high-pressure systems. We then use the maximum observed CO (1–0) size for each target as the lower bound error on pressure that is introduced from the CO observations. This uncertainty will be added in quadrature with other uncertainties to determine the lower limit of pressure for each target.

B.2. Stellar Velocity Dispersion

Based on results from Bassett et al. (2014), which compare the velocity dispersion of gas and stars in DYNAMO galaxies, we find that the standard approximation for stellar velocity dispersion, $\sigma_* \approx 1/2\sqrt{\pi G l_* \Sigma_*}$, where the disk scale length $l_* \approx R_{\text{half},*}/1.76$, reproduced measured velocities within $\pm 10 \text{ km s}^{-1}$. We also consider a simpler formulation where $\sigma_* \approx \sigma + 15 \text{ km s}^{-1}$. We find that these result in similar overall values of P when inserted into Equation (5). For the sake of consistency with previous studies (e.g., Leroy et al. 2008) we use $\sigma_* \approx 1/2\sqrt{\pi G l_* \Sigma_*}$. Note that, as done in Bassett et al. (2014), we assume that for DYNAMO galaxies $\sigma \approx \sigma_z$. More





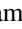
work on the stellar kinematics of turbulent disks would certainly be informative for these assumptions.

B.3. Total Gas Surface Density

A significant source uncertainty in the calculation of the midplane pressure is the estimation of the total gas mass surface density. Our observations of CO (1–0) only allow for observation of the molecular gas. However, estimations of midplane pressure refer to the entire gas mass surface density, atomic and molecular. Observing atomic gas masses on $z \sim 0.1$ galaxies is difficult with present facilities (Catinella & Cortese 2015) and is a primary goal of future SKA pathfinders. We caution that since the midplane pressure depends on Σ_{gas}^2 , even small differences in Σ_{gas} may significantly affect the slope of correlations.

We use a multistep method to estimate the total gas density. Observations of local spirals find that $\Sigma_{\text{atm}} \sim 5\text{--}10 M_{\odot} \text{pc}^{-2}$ (e.g., Bigiel et al. 2008). We first use a conservative estimate assuming the constant $\Sigma_{\text{atm}} \sim 5 M_{\odot} \text{pc}^{-2}$ to estimate the midplane pressure. Blitz & Rosolowsky (2006) give a correlation between the ratio of molecular to atomic gas, R_{mol} , and the total pressure, P/k . Using our initial estimate of pressure, which assumed $\Sigma_{\text{atm}} \sim 5 M_{\odot} \text{pc}^{-2}$, we then calculate the expected R_{mol} for DYNAMO galaxies. Note that in DYNAMO galaxies the stellar and molecular surface densities are more likely to drive the value of the pressure. We then recalculate the midplane pressure with the new estimate of $\Sigma_{\text{atm}} = \Sigma_{\text{mol}}/R_{\text{mol}}$. We find that for galaxies with high surface densities of gas ($\Sigma_{\text{mol}} \gtrsim 30 M_{\odot} \text{pc}^{-2}$) the difference in calculated midplane pressure (constant versus variable Σ_{atm}) is small, less than 0.01 dex. However, for the two lowest surface density galaxies in our sample the difference in pressures reaches 0.12 dex. This difference will be reflected in error bars in the associated figures. We rerun this estimation assuming the larger value of $\Sigma_{\text{atm}} = 15 M_{\odot} \text{pc}^{-2}$ as an initial guess. We find that this has at most a difference of 0.04 dex in determined pressure, and only on the two targets with the lowest Σ_{gas} .

ORCID iDs

D. B. Fisher  <https://orcid.org/0000-0003-0645-5260>
 A. D. Bolatto  <https://orcid.org/0000-0002-5480-5686>
 H. White  <https://orcid.org/0000-0001-7013-6921>
 K. Glazebrook  <https://orcid.org/0000-0002-3254-9044>
 R. G. Abraham  <https://orcid.org/0000-0002-4542-921X>

References

- Bassett, R., Glazebrook, K., Fisher, D. B., et al. 2014, *MNRAS*, 442, 3206
 Bassett, R., Glazebrook, K., Fisher, D. B., et al. 2017, *MNRAS*, 467, 239
 Bekiaris, G., Glazebrook, K., Fluke, C. J., & Abraham, R. 2016, *MNRAS*, 455, 754
 Benincasa, S. M., Wadsley, J., Couchman, H. M. P., & Keller, B. W. 2016, *MNRAS*, 462, 3053
 Bigiel, F., & Blitz, L. 2012, *ApJ*, 756, 183
 Bigiel, F., Leroy, A., Walter, F., et al. 2008, *AJ*, 136, 2846
 Blitz, L., & Rosolowsky, E. 2006, *ApJ*, 650, 933
 Boissier, S., Prantzos, N., Boselli, A., & Gavazzi, G. 2003, *MNRAS*, 346, 1215
 Bolatto, A. D., Warren, S. R., Leroy, A. K., et al. 2015, *ApJ*, 809, 175
 Bolatto, A. D., Wolfire, M., & Leroy, A. K. 2013, *ARA&A*, 51, 207
 Calzetti, D. 2001, *PASP*, 113, 1449
 Catinella, B., & Cortese, L. 2015, *MNRAS*, 446, 3526
 Combes, F., García-Burillo, S., Braine, J., et al. 2013, *A&A*, 550, A41
 Davé, R., Finlator, K., & Oppenheimer, B. D. 2011, *MNRAS*, 416, 1354
 Davies, R., Förster Schreiber, N. M., Cresci, G., et al. 2011, *ApJ*, 741, 69
 Dekel, A., Sari, R., & Ceverino, D. 2009, *ApJ*, 703, 785
 Dessauges-Zavadsky, M., & Adamo, A. 2018, *MNRAS*, 479, L118
 Dessauges-Zavadsky, M., Zamojski, M., Schaerer, D., et al. 2015, *A&A*, 577, A50
 Elmegreen, B. G. 1989, *ApJ*, 338, 178
 Elmegreen, B. G., & Efremov, Y. N. 1997, *ApJ*, 480, 235
 Elmegreen, D. M., Elmegreen, B. G., Rubin, D. S., & Schaffer, M. A. 2005, *ApJ*, 631, 85
 Faucher-Giguère, C.-A., Quataert, E., & Hopkins, P. F. 2013, *MNRAS*, 433, 1970
 Federrath, C., & Klessen, R. S. 2012, *ApJ*, 761, 156
 Fisher, D. B., Bolatto, A., Drory, N., et al. 2013, *ApJ*, 764, 174
 Fisher, D. B., Glazebrook, K., Abraham, R. G., et al. 2017a, *ApJL*, 839, L5
 Fisher, D. B., Glazebrook, K., Bolatto, A., et al. 2014, *ApJL*, 790, L30
 Fisher, D. B., Glazebrook, K., Damjanov, I., et al. 2017b, *MNRAS*, 464, 491
 Förster Schreiber, N. M., Genzel, R., Bouché, N., et al. 2009, *ApJ*, 706, 1364
 Gentry, E. S., Krumholz, M. R., Dekel, A., & Madau, P. 2017, *MNRAS*, 465, 2471
 Gentry, E. S., Krumholz, M. R., Madau, P., & Lupi, A. 2019, *MNRAS*, 483, 3647
 Genzel, R., Newman, S., Jones, T., et al. 2011, *ApJ*, 733, 101
 Genzel, R., Tacconi, L. J., Lutz, D., et al. 2015, *ApJ*, 800, 20
 Green, A. W., Glazebrook, K., Gilbank, D. G., et al. 2017, *MNRAS*, 470, 639
 Green, A. W., Glazebrook, K., McGregor, P. J., et al. 2010, *Natur*, 467, 684
 Green, A. W., Glazebrook, K., McGregor, P. J., et al. 2014, *MNRAS*, 437, 1070
 Guo, Y., Ferguson, H. C., Bell, E. F., et al. 2015, *ApJ*, 800, 39
 Guo, Y., Giavalisco, M., Ferguson, H. C., Cassata, P., & Koekemoer, A. M. 2012, *ApJ*, 757, 120
 Hao, C.-N., Kennicutt, R. C., Johnson, B. D., et al. 2011, *ApJ*, 741, 124
 Herrera-Camus, R., Bolatto, A., Wolfire, M., et al. 2017, *ApJ*, 835, 201
 Hodge, J. A., Riechers, D., Decarli, R., et al. 2015, *ApJL*, 798, L18
 Hopkins, A. M., & Beacom, J. F. 2006, *ApJ*, 651, 142
 Hopkins, P. F., Kereš, D., Oñorbe, J., et al. 2014, *MNRAS*, 445, 581
 Hopkins, P. F., Quataert, E., & Murray, N. 2011, *MNRAS*, 417, 950
 Inoue, S., & Yoshida, N. 2018, *MNRAS*, 474, 3466
 Isobe, T., Feigelson, E. D., Akritas, M. G., & Babu, G. J. 1990, *ApJ*, 364, 104
 Kennicutt, R. C. 1998, *ApJ*, 498, 541
 Kim, C.-G., Kim, W.-T., & Ostriker, E. C. 2011, *ApJ*, 743, 25
 Kim, C.-G., Ostriker, E. C., & Kim, W.-T. 2013, *ApJ*, 776, 1
 Kim, C.-G., Ostriker, E. C., & Raïleanu, R. 2017, *ApJ*, 834, 25
 Kim, J.-G., Kim, W.-T., & Ostriker, E. C. 2018, *ApJ*, 859, 68
 Krumholz, M. R., & Burkhardt, B. 2016, *MNRAS*, 458, 1671
 Krumholz, M. R., Burkhardt, B., Forbes, J. C., & Crocker, R. M. 2018, *MNRAS*, 477, 2716
 Krumholz, M. R., Dekel, A., & McKee, C. F. 2012, *ApJ*, 745, 69
 Krumholz, M. R., & McKee, C. F. 2005, *ApJ*, 630, 250
 Lagos, C. d. P., Crain, R. A., Schaye, J., et al. 2015, *MNRAS*, 452, 3815
 Larkin, J., Barczys, M., Krabbe, A., et al. 2006, *NewAR*, 50, 362
 Lehnert, M. D., Le Tiran, L., Nesvadba, N. P. H., et al. 2013, *A&A*, 555, A72
 Lehnert, M. D., Nesvadba, N. P. H., Le Tiran, L., et al. 2009, *ApJ*, 699, 1660
 Leroy, A. K., Bigiel, F., de Blok, W. J. G., et al. 2012, *AJ*, 144, 3
 Leroy, A. K., Walter, F., Brinks, E., et al. 2008, *AJ*, 136, 2782
 Levy, R. C., Bolatto, A. D., Teuben, P., et al. 2018, *ApJ*, 860, 92
 Madau, P., & Dickinson, M. 2014, *ARA&A*, 52, 415
 Magdis, G. E., Rigopoulou, D., Daddi, E., et al. 2017, *A&A*, 603, A93
 Moiseev, A. V., Tikhonov, A. V., & Klypin, A. 2015, *MNRAS*, 449, 3568
 Murray, N., Ménard, B., & Thompson, T. A. 2011, *ApJ*, 735, 66
 Nanayakkara, T., Glazebrook, K., Kacprzak, G. G., et al. 2017, *MNRAS*, 468, 3071
 Narayanan, D., Krumholz, M., Ostriker, E. C., & Hernquist, L. 2011, *MNRAS*, 418, 664
 Narayanan, D., Krumholz, M. R., Ostriker, E. C., & Hernquist, L. 2012, *MNRAS*, 421, 3127
 Obreschkow, D., Glazebrook, K., Bassett, R., et al. 2015, *ApJ*, 815, 97
 Obreschkow, D., & Rawlings, S. 2009, *ApJL*, 696, L129
 Oliva-Altamirano, P., Fisher, D., Glazebrook, K., et al. 2018, *MNRAS*, 474, 522
 Ostriker, E. C., McKee, C. F., & Leroy, A. K. 2010, *ApJ*, 721, 975
 Ostriker, E. C., & Shetty, R. 2011, *ApJ*, 731, 41
 Rahman, N., Bolatto, A. D., Xue, R., et al. 2012, *ApJ*, 745, 183
 Robotham, A. S. G., & Obreschkow, D. 2015, *PASA*, 32, e033
 Saintonge, A., Kauffmann, G., Wang, J., et al. 2011, *MNRAS*, 415, 61
 Salim, D. M., Federrath, C., & Kewley, L. J. 2015, *ApJL*, 806, L36
 Sandstrom, K. M., Leroy, A. K., Walter, F., et al. 2013, *ApJ*, 777, 5
 Schinnerer, E., Groves, B., Sargent, M. T., et al. 2016, *ApJ*, 833, 112
 Scoville, N., Sheth, K., Aussel, H., et al. 2016, *ApJ*, 820, 83

- Shetty, R., & Ostriker, E. C. 2012, [ApJ](#), **754**, 2
- Speagle, J. S., Steinhardt, C. L., Capak, P. L., & Silverman, J. D. 2014, [ApJS](#), **214**, 15
- Spilker, J. S., Marrone, D. P., Aravena, M., et al. 2016, [ApJ](#), **826**, 112
- Swinbank, A. M., Harrison, C. M., Trayford, J., et al. 2017, [MNRAS](#), **467**, 3140
- Swinbank, A. M., Papadopoulos, P. P., Cox, P., et al. 2011, [ApJ](#), **742**, 11
- Swinbank, A. M., Smail, I., Sobral, D., et al. 2012, [ApJ](#), **760**, 130
- Tacconi, L. J., Genzel, R., Saintonge, A., et al. 2017, [arXiv:1702.01140](#)
- Tacconi, L. J., Neri, R., Genzel, R., et al. 2013, [ApJ](#), **768**, 74
- Toomre, A. 1964, [ApJ](#), **139**, 1217
- Übler, H., Genzel, R., Tacconi, L. J., et al. 2018, [ApJL](#), **854**, L24
- Walter, F., Brinks, E., de Blok, W. J. G., et al. 2008, [AJ](#), **136**, 2563
- White, H. A., Fisher, D. B., Murray, N., et al. 2017, [ApJ](#), **846**, 35
- Wisnioski, E., Förster Schreiber, N. M., Wuyts, S., et al. 2015, [ApJ](#), **799**, 209
- Wisnioski, E., Glazebrook, K., Blake, C., et al. 2012, [MNRAS](#), **422**, 3339